Electronic Supplementary Information

Graphitic carbon nitride quantum dots decorated three-dimension graphene as an efficient metal-free electrocatalyst for triiodide reduction

Hong Yuan,[a,†] Jia Liu,[a,†] Hansheng Li,[a,*] Yongjian Li,[a] Xiufeng Liu,[a] Daxin Shi,[a] Qin Wu[a] and Qingze Jiao[a,b,*]

[a] *School of Chemistry and Chemical Engineering, Beijing Institute of Technology, Beijing, 100081, China.*

[b] *School of Chemical Engineering and Materials Science, Beijing Institute of Technology, Zhuhai, 519085, China.*

Experimental

Synthesis of three-dimensional graphene

Graphene oxide (GO) was prepared from natural graphite powder by using a modified Hummers method[1] referring to our previous literature.[2, 3] 2 mL of GO dispersion (10 mg mL^{-1}) was dissolved into 40 mL ethanol under ultrasonic treatment for 30 min, and then centrifuged for 10 min. After that, the as-obtained mixture was transferred into a 55 ml Teflon-lined stainless steel autoclave for hydrothermal reaction at 180 °C for 24 h. The resultants were further diluted into deionized water and then freeze-dried for 48 h to obtain the black 3DG products.

Preparation of g-C_3N_4 QDs

Bulk g-C_3N_4 was prepared by directly pyrolysis condensation of melamine at 600 °C for 2 hours with a heating rate of 3 °C min^{-1}. Then 1g of bulk g-C_3N_4 was dispersed into the mixture of concentrated sulfuric acid (H_2SO_4) (20 mL) and nitric acid (HNO_3) (20 mL) at room temperature under stirring until a homogeneous solution was formed. Next, the solution was diluted with deionized water and washed for several times to obtain white products. Subsequently, 0.1 g of white product was dissolved into 40 mL $NH_3 \cdot H_2O$, and further the resulting suspension was sealed in a Teflon-lined autoclave and heated at 180 °C for 12 h. Upon cooling down to the room temperature, the resultant solution was treated by rotary evaporator to remove $NH_3 \cdot H_2O$ for obtaining some precipitates. Finally, the collected precipitates were diluted in deionized water and ultrasonicated for 6 h, followed by a high-speed centrifugation to achieve the aqueous dispersion of g-C_3N_4 QDs.[4]

Preparation of g-C_3N_4 QD@3DG nanocomposites

In a typical experiment process, 2 mL of GO dispersion (10 mg mL^{-1}) was dissolved into 40 mL ethanol, and the mixture was placed into a sonic bath for 30 min and further recovered using centrifugation for 10 min. Then the 2 mL g-C_3N_4 QDs aqueous dispersion (0.5 mg mL^{-1}) was slowly poured and intensely stirred for 30 min at room temperature. The mixed solution was

sealed into a 55 mL Teflon-lined autoclave and hydrothermally treated at 180 °C for 24 h. Finally, the resultant products were soaked into deionized water and stabilized, and then freeze-dried for 48 h to get the black g-C_3N_4 QD@3DG hybrids.

For comparison, the g-C_3N_4 particle@3DG hybrids are also prepared. The preparation process are as follows. First, the g-C_3N_4 particles are by the grinding treatment and subsequent ultrasound process. Then, preparation process of g-C_3N_4 particle@3DG are similar to that of g-C_3N_4 QD@3DG by replacing g-C_3N_4 QD with g-C_3N_4 particle.

Fabrication of CEs

About 10 mg of the as-synthesized materials, including pristine g-C_3N_4, 3DG, g-C_3N_4 particle@3DG and g-C_3N_4 QD@3DG hybrids, were dispersed into the mixture solvent of terpilenol and ethyl alcohol with 1 mg ethyl cellulose and grinded for 30 min to obtain the homogenous slurries. Afterwards, the electrode slurries were coated onto the FTO conductive substrates by using doctor-blade method and further dried in vacuum at 120 °C, then heated at 300 °C for 3 hours in nitrogen to serve as CEs. As a control, Pt CE was also prepared by the pyrolyzation of a drop of 20 mM H_2PtCl_6 ethanol solution onto FTO conductive substrate, followed by sintering at 400 °C for 15 min in air.

Fabrication of DSSCs

The TiO_2 pastes with the average size of 20 nm was coated on the FTO substrate and dried at 125 °C for 5 min, followed by screen printing TiO_2 pastes with particle size of 400 nm as a light scattering film on the coated TiO_2 layer. The as-prepared TiO_2 film was again annealed at 450 °C and 500 °C for 15 min in air, respectively. After cooling to room temperature, the TiO_2 film was immersed into a 0.5 mM N719 dye solution with a mixed solvent of acetonitrile and tert-butyl alcohol (volume ratio of 1:1) for 24 h to form the dye-sensitized photoanode. The work electrolyte was prepared with 0.6 M 1, 2-dimethyl-3-propylimidazolium iodide (DMPII), 0.06 M LiI, 0.03 M I_2 and 0.5 M 4-tert-butyl pyridine in acetonitrile solution. Finally, the sandwich structured DSSCs composed of a TiO_2 photoanode, different CEs and an interlayer spacer of a 30 μm-thick Surlyn film (Solaronix) were assembled.

Structural and electrochemical characteristics

The morphologies of all the samples were examined by the Field-emission scanning electron microscope (Hitachi S-4800) and transmission electron microscopy (JEM-2100, JEOL, Japan). XRD patterns were recorded using Ultima IV X-ray diffractometer (Rigaku, Japan) with CuKa radiation. Raman spectroscopy measurements were conducted on a Renishaw inVia-Reflex Raman Microscope with an excitation wavelength of 532 nm. Fourier transform infrared spectrometry (FT-IR) analysis was performed by using Nicolet iS10 Fourier transform infrared spectrometer (Thermo scientific, America). N_2 adsorption-desorption isotherm was determined by using Autosorb-IQ2-MP-C BET surface area analyzer. The chemical compositions of the as-made samples were investigated by X ray photoelectron spectroscopy (XPS) measurements conducted on a MULT1LAB2000VG photoelectron spectrometer.

The Electrochemical impedance spectra (EIS) and Tafel polarization were measured on a symmetric dummy cell by using electrochemical working station (CHI 604 E) under the dark condition. Cyclic voltammetry (CV) data were obtained with three-electrode configurations, by

using the as-prepared electrodes as the working electrode, platinum foil as the counter electrode, and Ag/AgCl electrode as the reference electrode in acetonitrile solution, consisting of 0.1 M $LiClO_4$, 10 mM LiI and 1 mM I_2. Photocurrent-photovoltage (J-V) characteristics of the DSSCs were evaluated under 100 mW cm^{-2} with AM 1.5 illuminations (Zolix SS150), which was calibrated by using a Si solar cell (National Institute of Metrology, China).

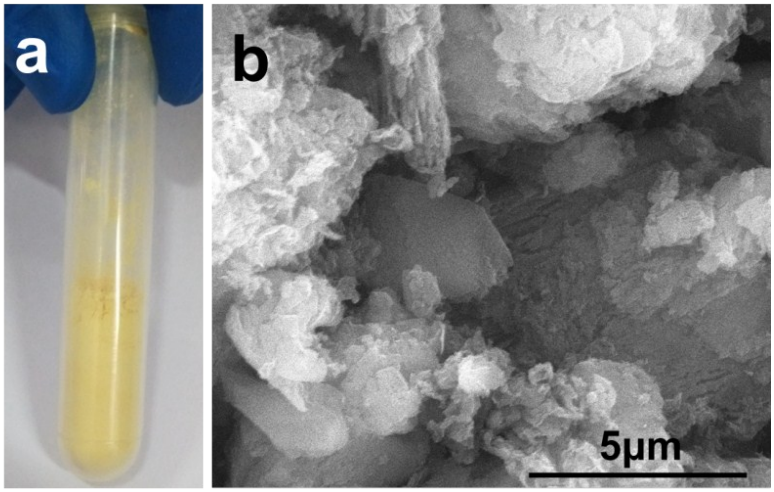

Fig. S1 (a) Optical photograph and (b) SEM image of the bulk g-C_3N_4 particles.

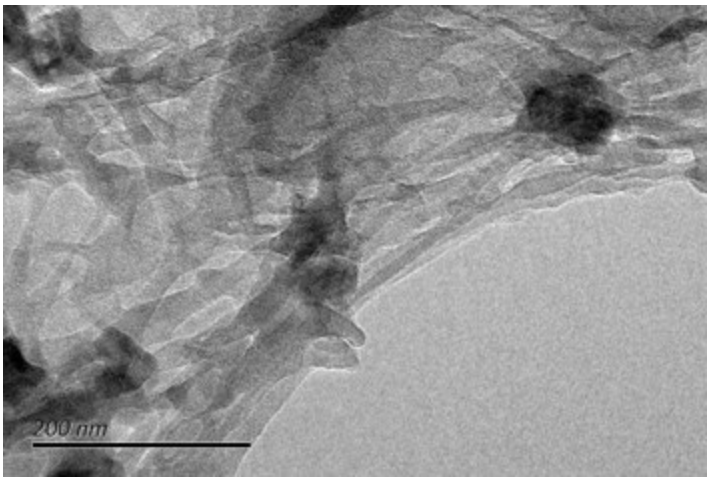

Fig. S2 TEM image of the as-prepared porous g-C_3N_4.

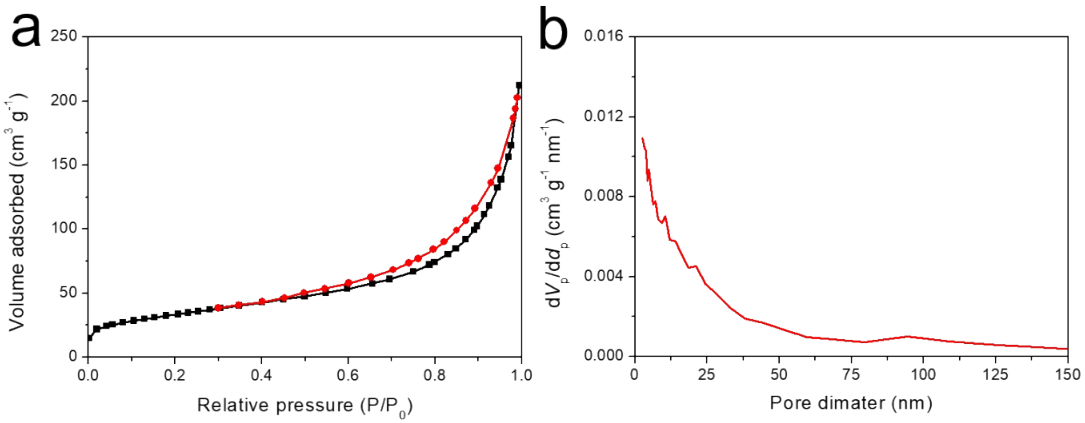

Fig. S3 (a)Nitrogen adsorption–desorption isotherms and (b) pore size distribution of g-C_3N_4 QD@3DG hybrids.

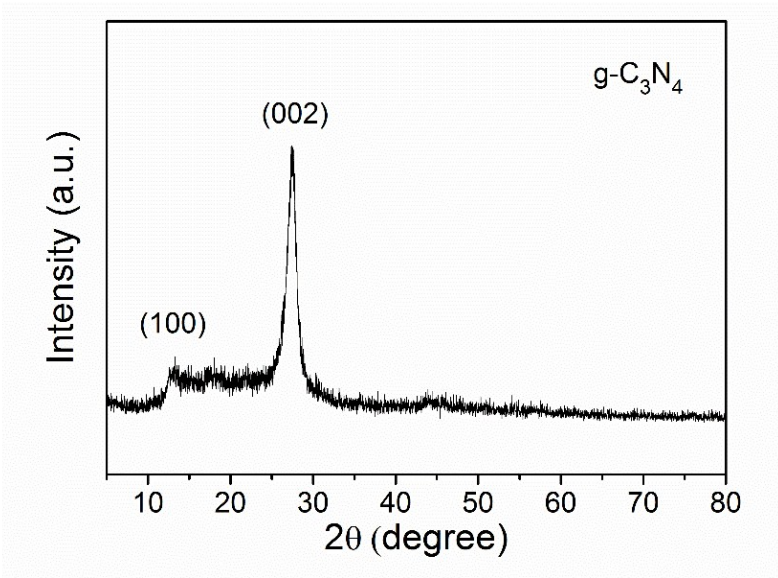

Fig. S4 XRD patterns of the bulk g-C_3N_4.

According to XRD analysis (Fig. S4), the as-prepared bulk g-C_3N_4 sample clearly reveals two characteristic diffraction peaks, in line with its (002) plane related to the inter-planar stacking peak of conjugated aromatic systems and (100) plane attributed to the in-plane structural motif between nitride pores.[5]

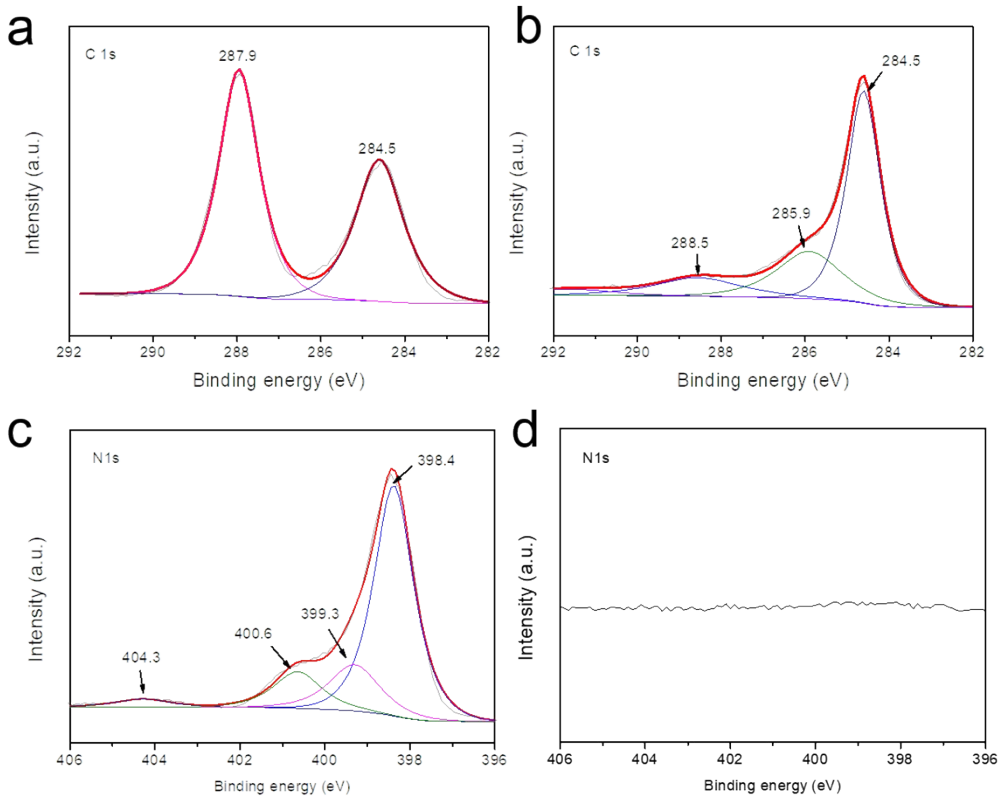

Fig. S5 (a and b) High resolution XPS spectra of C 1s for g-C_3N_4 and 3DG, (c and d) High resolution XPS spectra of N 1s for g-C_3N_4 and 3DG.

Fig. S5 shows the high resolution XPS spectra of C 1s and N 1s for g-C_3N_4 and 3DG, respectively. As shown in Fig. S5a, the C 1s spectrum of g-C_3N_4 displays two typical peaks: the first peak located at 284.5 eV belongs to the C=C, while the second peak at 287.9 eV can be assigned to sp^2-bonded carbon of g-C_3N_4 (N–C=N). In addition, for the 3DG samples, the high resolution C 1s spectrum (Fig. S5b) can be divided into three major peaks: (1) C=C coordination at 284.5 eV, (2) C-O bond at 285.9 eV) and (3) C=O-O bond at 288.5 eV. The N 1s spectrum for g-C_3N_4 (Fig. S5c) reveals the existence of sp^2 hybridized aromatic N at 398.4 eV, the tertiary N in tri-*s*-triazine units at 399.3 eV, amino N–H bonds at 400.6 eV and the g-C_3N_4 heterocycles with positive charge at 404.3 eV. notably, the N 1s spectrum for 3DG has not been detected (Fig. S5d), successfully demonstrating that N atoms are not actually exist in the 3DG samples.

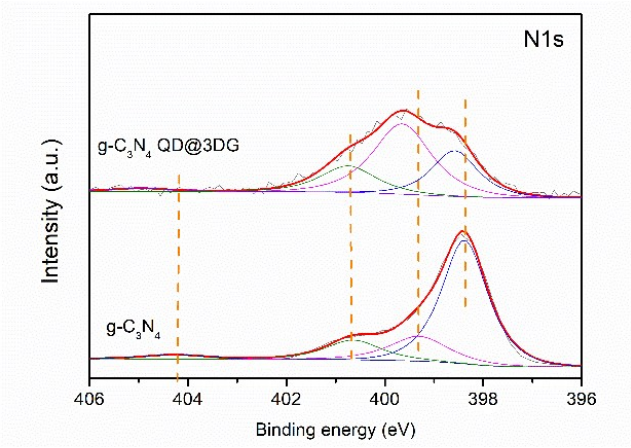

Fig. S6 Comparative XPS spectra of N 1s for g-C_3N_4 QD@3DG hybrids and pristine g-C_3N_4.

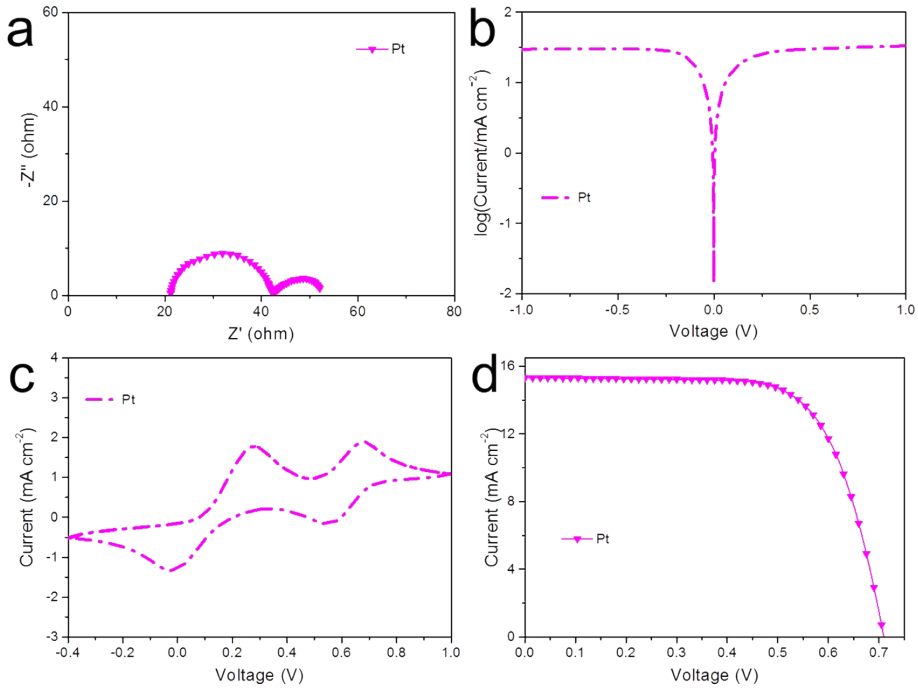

Fig. S7 (a) Nyquist plots, (b) Tafel polarization curves, (c) CV curves and (d) *J-V* curves of Pt CEs.

Table S1 Detailed photovoltaic parameters and EIS parameters of controlled Pt CE

	V_{oc} (V)	J_{sc} (mA cm^{-2})	FF	PCE (%)	R_s (Ω)	R_{ct} (Ω)
Pt	0.709	15.32	0.70	7.59	21.23	10.5

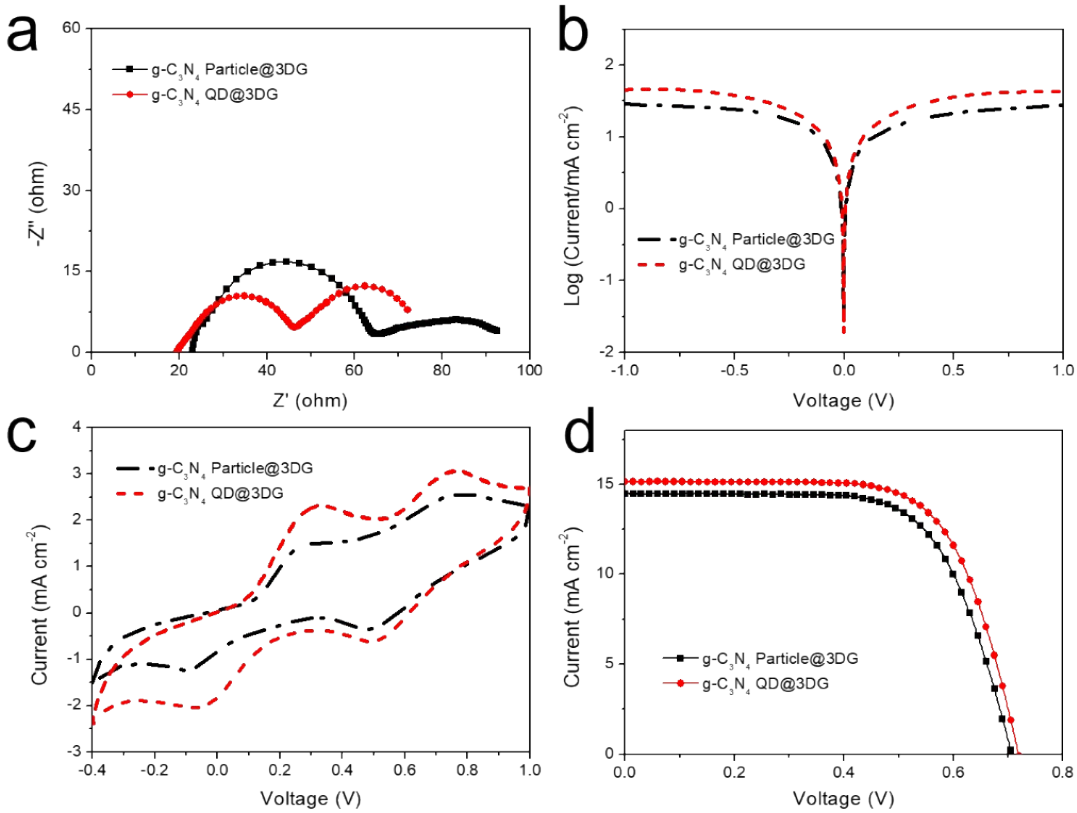

Fig. S8 (a) Nyquist plots, (b) Tafel polarization curves, (c) CV curves of g-C_3N_4 QD@3DG and g-C_3N_4 particle@3DG CEs; (d) *J-V* curves of DSSCs with above different CEs.

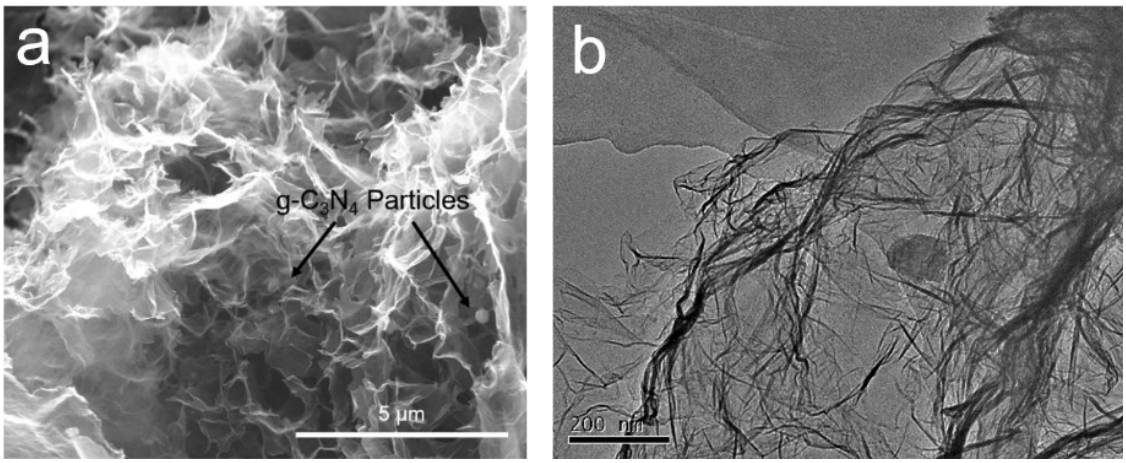

Figure S9 (a) SEM and (b) TEM images of g-C_3N_4 particle@3DG.

Table S2 Comparative performance characteristics of counter electrode materials in DSSCs with efficiency values and the reference Pt cell reported in the same paper

Counter electrode	Characteristic	Dye	Electrolyte	PCE, CE (%)	PCE, Pt (%)	Ref.
g-C_3N_4 QD@3DG	Metal-free	N719	I^-/I^{3-}	7.46	7.59	This work
g-C_3N_4/Graphene	Metal-free	N3	I^-/I^{3-}	7.13	7.37	6
g-C_3N_4/MWCNT (g-C_3N_4/multiwalled carbon nanotubes)	Metal-free	N3	I^-/I^{3-}	6.34	6.84	7
g-C_3N_4/CCB (g-C_3N_4/conductive carbon black)	Metal-free	N3	I^-/I^{3-}	5.09	5.45	8
SWCNH (Single wall carbon nanohorns)	Metal-free	N719	I^-/I^{3-}	4.09	5.71	9
CNP (Graphene nanoplatelets)	Metal-free	N719	I^-/I^{3-}	3.13	5.71	9
CNF-LSA (antler carbon nanofibers)	Metal-free	N719	I^-/I^{3-}	7.0	7.1	10
CNF-100 (herringbone carbon nanofiber)	Metal-free	N719	I^-/I^{3-}	6.8	7.1	10
Triton X-100/MWCNTs	Metal-free	N719	I^-/I^{3-}	2.69	4.35	11
HC-GCF (Graphene coated cotton fabric)	Metal-free	N719	I^-/I^{3-}	6.93	8.44	12
NPGFs (Nitrogen-doped porous graphene foams)	Metal-free	N719	I^-/I^{3-}	4.5	4.9	13
Poly(triazine imide) g-CN (graphitic carbon nitride)	Functionalized carbonaceous material	N719	I^-/I^{3-}	7.8	7.9	14
E-RGO (electrochemically reduced graphene oxide)	Functionalized carbonaceous material	MK-2	Co-based	5.07	5.10	15
MWCNT-PANI (Multi-walled carbon nanotubes-polyaniline)	Functionalized carbonaceous material	N719	I^-/I^{3-}	4.58		16
MWCNT-PANI-Ni^{2+}	Metal doped carbonaceous material	N719	I^-/I^{3-}	6.0		16
N-OCMCs (N-doped ordered cubic mesoporous carbons)	Metal doped carbonaceous material	N719	I^-/I^{3-}	5.60	6.46	17
NGnP (P-doped rGO)	Metal doped carbonaceous material	N719	I^-/I^{3-}	6.04	6.80	18
OMC/GNS (ordered mesoporous carbon / graphene nano-sheets)	Metal-free	N719	I^-/I^{3-}	6.82	7.08	19
NPC (N/P co-doped carbon	Metal doped carbonaceous	N719	I^-/I^{3-}	6.74	5.76	20

nanosheets)	material					
CNx/CNTs (Nitrogen-doped carbon/ carbon nanotubes)	Metal doped carbonaceous material	N719	I^-/I^{3-}	7.38	7.13	21
Graphene/FTO	Graphene composites	N719	I^-/I^{3-}	9.03	9.07	22
FGNS-CoS (functionalized graphene Nanosheets-CoS)	Metal compounds - graphene composites	N719	I^-/I^{3-}	5.54	5.90	23
TiS_2–G	Metal compounds - graphene composites	N719	I^-/I^{3-}	8.80	8.0	24
SRO–GQD ($SrRuO_3$-graphene quantum dots)	Metal oxides - graphene composites	N719	I^-/I^{3-}	8.05	7.44	25
Fe_2O_3/GFs	Metal oxides - graphene composites	N719	I^-/I^{3-}	7.45	7.29	26

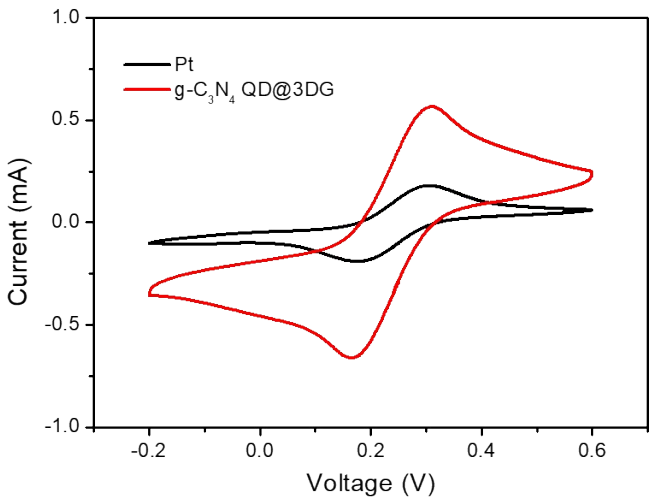

Fig. S10 CV curves of g-C_3N_4 QD@3DG and controlled Pt samples in 5 mM $K_3Fe(CN)_6$/0.1 M KCl solution (scan rate: 50 mV s^{-1}).

Table S3 Calculated electroactive surface areas for g-C_3N_4 QD@3DG and Pt samples

CEs	g-C_3N_4 QD@3DG	Pt
Electroactive surface area (cm^2)	1.056	0.303

The electrochemical active area (ECA) for the g-C_3N_4 QD@3DG and Pt samples are measured through cyclic voltammetry (CV) curves in 5 mM $K_3Fe(CN)_6$/0.1 M KCl solution, of which the results are shown in Fig. S10. The ECA was calculated using the Randles-Sevcik equation:

$$A = \frac{I_P}{2.69 \times 10^5 \times n^{3/2} \times D^{1/2} \times V^{1/2} \times C}$$

Where, A is the electroactive surface area (cm^2), I_p is the peak current (A), n is the electron transfer number, here, n=1, D is the diffusion coefficient of the solute, D=4.34×10^{-6} (cm^2 s^{-1}), V is the scan rate (V s^{-1}), and V = 0.05 V s^{-1}, C is the concentration (mol mL^{-1}).

In this work, the tested area is 0.1256 cm^2 (3.14×0.2×0.2 cm^2). Thus, according to the equation above, the electroactive surface areas of different counter electrodes are calculated and the corresponding results are listed in Table S3. The ECA of g-C_3N_4 QD@3DG is 1.056 cm^2, much higher than that of Pt sample (0.303 cm^2), which can expose more active sites and enhance the contact between g-C_3N_4 QD@3DG electrode and electrolyte, thus contributing to a high photovoltaic efficiency in DSSCs.

Reference

1 W. S. Hummers Jr and R. E. Offeman, J. Am. Chem. Soc., 1958, **80**, 1339-1339.

2 H. Yuan, J. Liu, Q. Jiao, Y. Li, X. Liu, D. Shi, Q. Wu, Y. Zhao and H. Li, Carbon, 2017, **119**, 225-234.

3 H. Yuan, Q. Jiao, J. Liu, X. Liu, H. Yang, Y. Zhao, Q. Wu, D. Shi and H. Li, J. Power Sources, 2016, **336**, 132-142.

4 X. D. Zhang, H. X. Wang, H. Wang, Q. Zhang, J. F. Xie, Y. P. Tian, J. Wang and Y. Xie, Adv. Mater., 2014, **26**, 4438-4443.

5 C. Xu, Q. Han, Y. Zhao, L. Wang, Y. Li and L. Qu, J. Mater. Chem. A, 2015, **3**, 1841-1846

6 G. Wang, J. Zhang, S. Kuang and W. Zhang, *Chem. Eur. J.*, 2016, **22**, 11763-11769.

7 G. Wang, S. Kuang, J. Zhang, S. Hou and S. Nian, *Electrochim. Acta*, 2016, **187**, 243-248.

8 G. Wang, J. Zhang and S. Hou, *Mater. Res. Bull.*, 2016, **76**, 454-458.

9 K. Susmitha, M. M. Kumari, A. J. Berkmans, M. N. Kumar, L. Giribabu, S. Manorama and M. Raghavender, *Sol. Energy*, 2016, **133**, 524-532.

10 G. Veerappan, W. Kwon and S.-W. Rhee, *J. Power Sources*, 2011, **196**, 10798-10805.

11 J. Zhao, J. Ma, X. Nan and B. Tang, *Org. Electron.*, 2016, **30**, 52-59.

12 I. A. Sahito, K. C. Sun, A. A. Arbab, M. B. Qadir, Y. S. Choi and S. H. Jeong, *J. Power Sources*, 2016, **319**, 90-98.

13 L. Song, Q. Luo, F. Zhao, Y. Li, H. Lin, L. Qu and Z. Zhang, *Phys. Chem. Chem. Phys.*, 2014, **16**, 21820-21826.

14 W. r. Lee, Y. S. Jun, J. Park and G. D. Stucky, *J. Mater. Chem. A*, 2015, **3**, 24232-24236.

15 S. H. Seo, E. J. Jeong, J. T. Han, H. C. Kang, S. I. Cha, D. Y. Lee and G.-W. Lee, *ACS Appl. Mater. Interfaces*, 2015, **7**, 10863-10871.

16 K. Wu, L. Chen, C. Duan, J. Gao and M. Wu, *Mater. Design*, 2016, **104**, 298-302.

17 M. Chen, L. L. Shao, Y.-P. Liu, T. Z. Ren and Z. Y. Yuan, *J. Power Sources*, 2015, **283**, 305-313.

18 Z. Wang, P. Li, Y. Chen, J. He, J. Liu, W. Zhang and Y. Li, *J. Power Sources*, 2014, **263**, 246-251.

19 L.L. Shao, M. Chen, T. Z. Ren and Z. Y. Yuan, *J. Power Sources*, 2015, **274**, 791-798.

20 M. Chen, L. L. Shao, Y. X. Guo and X. Q. Cao, *Chem. Eng. J.*, 2016, **304**, 303-312.

21 A. Shrestha, M. Batmunkh, C. J. Shearer, Y. Yin, G. G. Andersson, J. G. Shapter, S. Qiao and S. Dai, *Adv.Energy Mater.*, 2017, **7**, 1602276-1602283.
22 M. W. Lee, H.-Y. Kim, H. Yoon, J. Kim and J. S. Suh, Carbon, 2016, **106**, 48-55.
23 X. Miao, K. Pan, G. Wang, Y. Liao, L. Wang, W. Zhou, B. Jiang, Q. Pan and G. Tian, *Chem. Eur. J.*, 2014, **20**, 474-482.
24 X. Meng, C. Yu, B. Lu, J. Yang and J. Qiu, *Nano Energy*, 2016, **22**, 59-69.
25 T. Liu, K. Yu, L. Gao, H. Chen, N. Wang, L. Hao, T. Li, H. He and Z. Guo, *J. Mater. Chem. A*, 2017, **5**, 17848-17855.
26 W. Yang, X. Xu, Z. Li, F. Yang, L. Zhang, Y. Li, A. Wang and S. Chen, Carbon, 2016, **96**, 947-954.